A Century of Stability of Avannarleq and Kujalleq Glaciers, West Greenland, Explained Using High-Resolution Airborne Gravity and Other Data

L. An[1] [ID], E. Rignot[1,2] [ID], J. Mouginot[1] [ID], and R. Millan[1] [ID]

[1] Department of Earth System Science, University of California, Irvine, CA, USA, [2] Jet Propulsion Laboratory, California Institute of Technology, Pasadena, CA, USA

Abstract The evolution of Greenland glaciers in a warming climate depends on their depth below sea level, flow speed, surface melt, and ocean-induced undercutting at the calving front. We present an innovative mapping of bed topography in the frontal regions of Sermeq Avannarleq and Kujalleq, two major glaciers flowing into the ice-choked Torssukatak Fjord, central west Greenland. The mapping combines a mass conservation algorithm inland, multibeam echo sounding data in the fjord, and high-resolution airborne gravity data at the ice-ocean transition where other approaches have traditionally failed. We obtain a reliable, precision (± 40 m) solution for bed topography across the ice-ocean boundary. The results reveal a 700 m deep fjord that abruptly ends on a 100–300 m deep sill along the calving fronts. The shallow sills explain the presence of stranded icebergs, the resilience of the glaciers to ocean-induced undercutting by warm Atlantic water, and their remarkable stability over the past century.

1. Introduction

Marine-terminating glaciers control 88% of the ice discharge of Greenland into the ocean (Rignot & Mouginot, 2012) and have a major impact on the evolution of the Greenland Ice Sheet mass balance (van den Broeke et al., 2009). These glaciers have been thinning over the 1990s (Krabill, 2000), due to change in ice dynamics triggering a process of thinning, acceleration, and retreat (Luckman & Murray, 2005; Lüthi et al., 2016; Thomas et al., 2000). Warm air temperatures thin the glaciers from the top and melt the ice mélange (sea ice and iceberg debris) in front of them, while warm, salty, subsurface ocean water of Atlantic origin (AW) erodes the mélange from the bottom and undercuts the submerged glacier faces, causing calving and grounding line retreat (Holland et al., 2008; Rignot, Fenty, et al., 2016; Straneo et al., 2013).

The impact of ice melt by the ocean depends on the access of subsurface (>300 m) AW to the glacier fronts (Rignot, Xu, et al., 2016) and the depth of the glacier fronts. As the glaciers retreat in response to enhanced melt, the rate and extent of the retreat will depend on the shape of the bed. If the glacier retreats along a reverse bed, that is, where bed elevation drops in the inland direction, the retreat will proceed rapidly and irreversibly even if the climate returns to a colder state (Meier & Post, 1987; Thomas, 1979; Weertman, 1974). This process is known as the tidewater glacier cycle or marine ice sheet instability (Pfeffer, 2007). In contrast, if the glacier retreat proceeds along a normal bed, where bed elevation rises in the inland direction, the retreat will proceed more slowly or may stop.

Glacier front regions are challenging to survey. Bed mapping using airborne radio echo sounding (RES) is notoriously difficult in entrenched terminal valleys due to ambiguous radar echoes from the sides, multiple returns from a broken-up glacier surface that generate high radar clutter, warm ice temperature that yield high absorption of radar signals, and water inclusions conducive to enhanced scattering of the radar signals. Hence, few bed picks from RES data are available to constrain the bed elevation of many Greenland marine-terminating glaciers near their calving fronts (Gogineni et al., 2014). Reliable RES data are found many tens of kilometers upstream of ice fronts.

To circumvent this limitation, a mass conservation (MC) approach has been developed that combines ice thickness data derived from RES data in the upstream region, ice motion vectors from synthetic-aperture radar and optical remote sensing, reconstructions of surface mass balance (SMB) from regional atmospheric climate models, and estimates of ice thinning from altimetry data. MC combines these data using a cost minimization
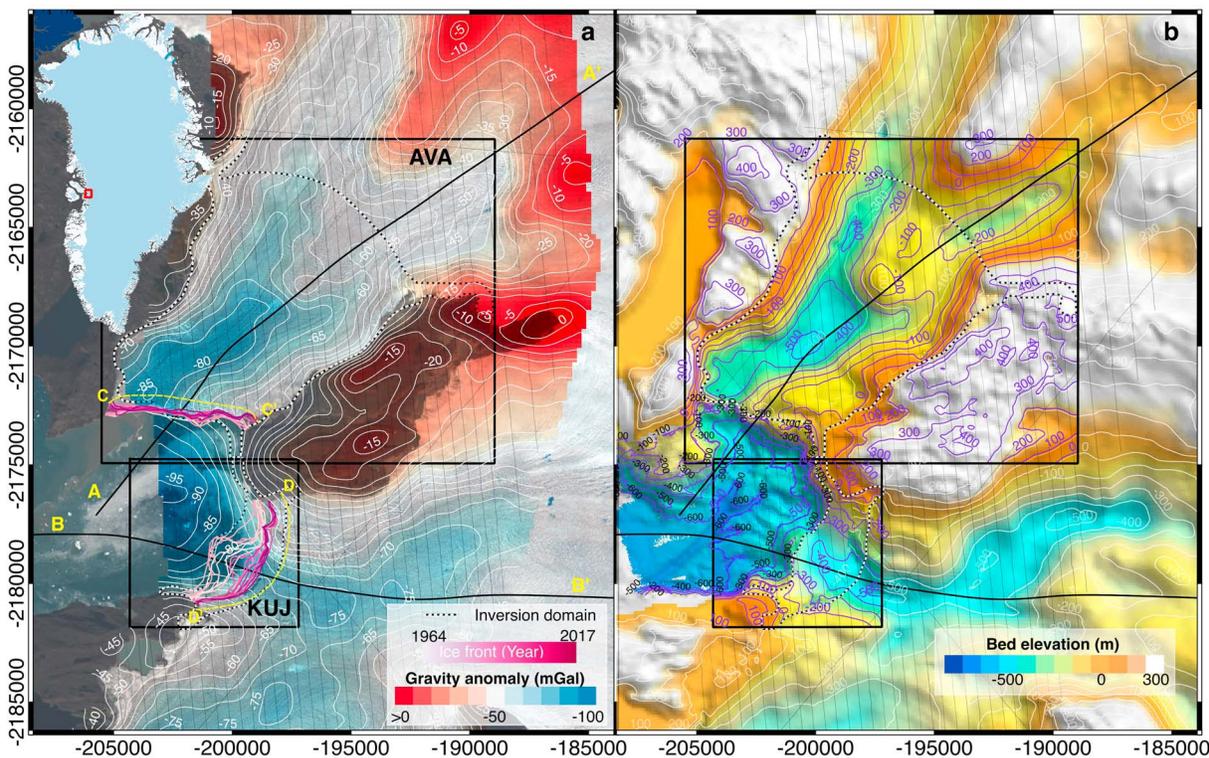
Figure 1. (a) Airborne, high-resolution, free-air gravity anomalies of Sermeq Avannarleq (AVA) and Kujalleq (KUJ), Greenland in milligal (1 mGal = 10⁻⁵ m²/s) with 5 mGal contours in white, overlaid on a Landsat-8 image. Survey lines are thin black lines. Ice front positions are color coded from light (1964) to deep pink (2017). (b) Bed elevation and fjord bathymetry color coded from white to orange (300 m to 0 m depth) to green, blue, and dark blue (100 to 800 m depth) with 100 m contours in white and purple. Gravity inversion domain is thin white-black dash lines. Profile AA′ and BB′ are shown in Figure 2.

approach to reconstruct an ice thickness map at 150 m spacing that conserves mass, known as BedMachineV3 or BM3 (Morlighem et al., 2014, 2017). Bed elevation is deduced as surface elevation minus ice thickness. The error in reconstructed bed elevation accumulates in the downstream direction with the distance from the control ice thickness data and hence is largest at the ice fronts.

At sea, the depth of many glacial fjords was not known until multibeam echo sounder (MBES) surveys of the late 2000s (Rignot, Fenty, et al., 2016). Where MBES data exist and extend to the base of the ice fronts, the MC approach has been modified to provide a seamless transition with MBES data at the ice-ocean boundary (Morlighem et al., 2017). Access of ships to the glacier fronts, however, is often difficult due the ubiquitous presence of stranded iceberg debris in front of the glaciers, and the unpredictable and dangerous nature of calving events. Shipborne surveys leave data gaps of many kilometers near the ice fronts, so that the MC method cannot constrain the bed solution at the ice front and uncertainties in bed elevation remain large, possibly several hundreds of meters. Such large errors make it difficult to constrain the output fluxes from the glaciers, understand how warm ocean waters access the glacier fronts, or constrain the geometry of the bed to reproduce or understand the evolution of the glaciers in a warming climate.

Here we present an approach to fill the gap between land and sea floor surveys using high-resolution, high-precision airborne gravity data. The gravity data were collected in August 2012 on board a low-flying, low-speed, helicopter using the Sander Geophysics Ltd (SGL) Airborne Inertially Referenced Gravimeter (AIRGrav) (Argyle et al., 2000). The survey covers two major outlet glaciers of central west Greenland: Sermeq Avannarleq (AVA) and Kujalleq (KUJ) (Figures 1 and 2). These glaciers flow into the ice-choked Torssukatak Fjord. We use a 3-D inversion of the gravity data constrained by MBES data at sea and BM3 inland. We evaluate the precision and uncertainty of the inferred bed elevation and compare the results with earlier mappings. We discuss the impact of our mapping on the understanding of the recent and future evolution of major outlet glaciers.
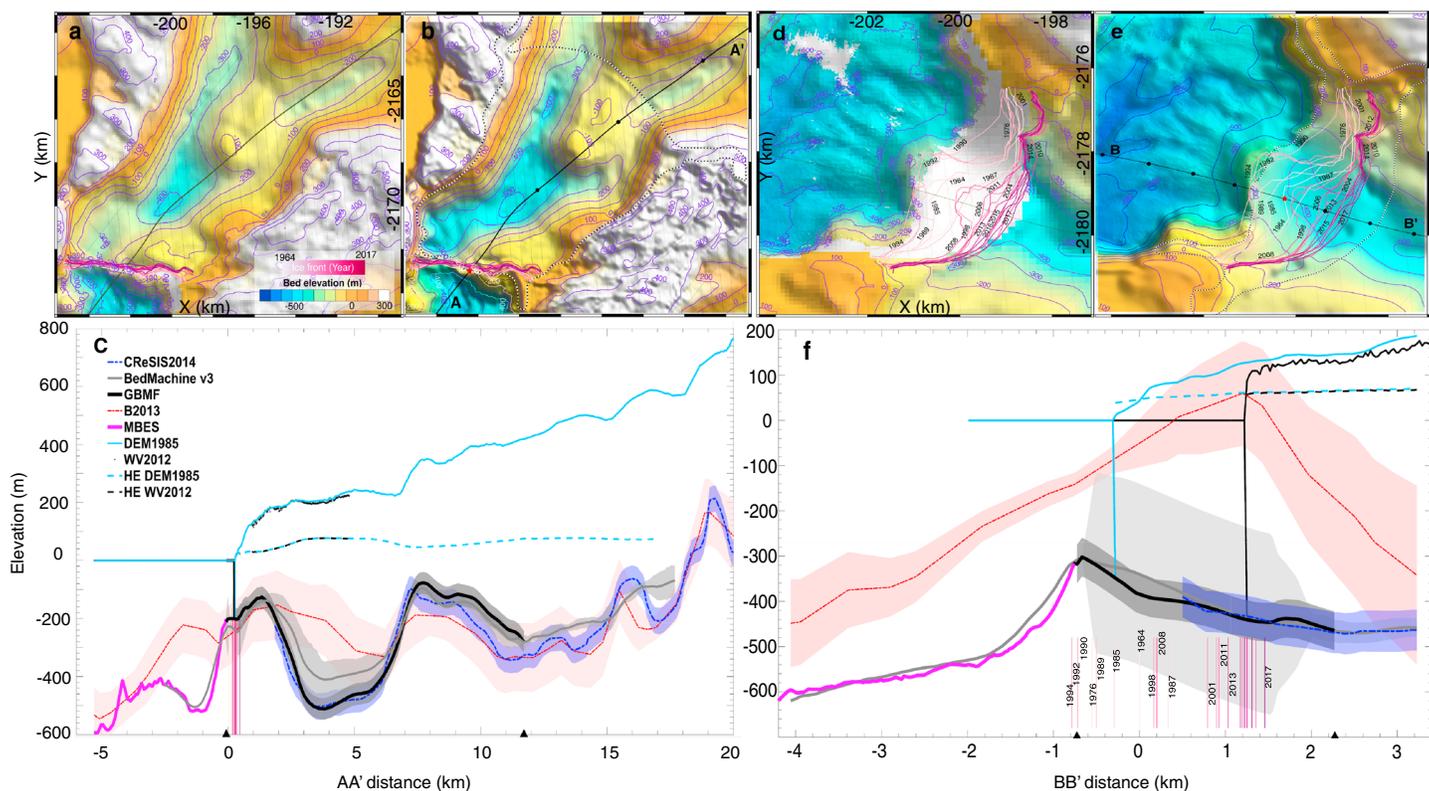
Figure 2. (a and d) Mass conservation bed elevation on land and multibeam echo sounding (MBES) in the ocean for Sermeq Avannarleq and Kujalleq, Greenland. (b and e) Bed elevation from gravity color coded from white to orange (300 m to 0 m) to green, blue, and dark blue (100 to 800 m depth) with 100 m contours in purple. Profile AA′ and BB′ are CReSIS RES data from 14 April 2014 and 6 April 2013, respectively (Figure S4). Black circles indicate 5 km intervals from the 1964 ice front (red star) of Sermeq Avannarleq and 1 km intervals for Kujalleq. (c and f) Glacier surface and bed elevation from this study are thick black lines with errors in dark gray, BM3 (Morlighem et al., 2017) is light gray, CReSIS is blue, Bamber et al. (2013) is red, and MBES is magenta. Black triangles indicate the limits of the gravity inversion.

2. Data and Methods

2.1. Glacier Setting

Sermeq Avannarleq AVA (70°3′N, 50°19′W) and Kujalleq KUJ (69°59′N, 50°10′W) are marine-terminating glaciers in central West Greenland (Figure 1a) that drain areas of 7,958 km^2 and 18,263 km^2, respectively, with a sea level equivalent of 4.4 cm and 10.9 cm based on BM3. Their balance discharges are 1.5 and 5.6 Gt/yr, respectively, based on the average SMB for the years 1961–1990 from RACMO2.3 (Ettema et al., 2010). AVA flows at a center speed of 1.5 km/yr at the ice front (35th glacier in Greenland) versus 3.0 km/yr for KUJ (16th glacier) (Rignot & Mouginot, 2012).

2.2. Glacier Speed and Ice Front Evolution

We obtain time series of ice front velocity using data from the U.S. Landsat series, the Japanese ALOS PALSAR: Advanced Land Observing Satellite Phased Array type L-band Synthetic Aperture Radar, the European ERS-1/2, the Canadian RADARSAT-1/2, and the European Sentinel-1a/b, spanning from the 1980s to 2017. Ice speed is averaged across the ice front to calculate an average speed across the glacier width, which is lower than the speed at the glacier center. The mean speed of AVA is 1,080 m/yr. We find significant seasonal fluctuations in speed, especially in recent years. The mean speed dropped by 10% from 1,180 ± 118 m/yr in 1985–2004 to 1,016 ± 200 m/yr in 2005–2017 (Figure 3). The mean speed of KUJ is 2,280 m/yr, increasing from 2,080 ± 190 m/yr in 1985–1998 to 2,548 ± 200 m/yr in 2000–2005 and dropping back to 2,075 ± 145 m/yr in 2005–2017.

We digitize the summer ice front positions using aerial photos from 1964 (Carbonnell & Bauer, 1968) and Landsat imagery spanning 1976 to 2017. AVA did not retreat at a significant level (150–200 m) during the entire time period (Figure 1). KUJ advanced and retreated over a region about 2.5 km wide. At midrange in the 1960s to 1970s, the ice front advanced in the 1980s, remained at an advanced position in the 1990s, and retreated by 1.5 km from 1997 to 2001. The ice front of KUJ has remained stable within ±300 m since 2001. On the longer term, AVA has not migrated more than 100 m since 1903, while KUJ retreated by 2 km in 1851–1949, followed by stable conditions in 1949–1961, and a readvance of 700 m in 1961–1964 (Weidick, 1968).
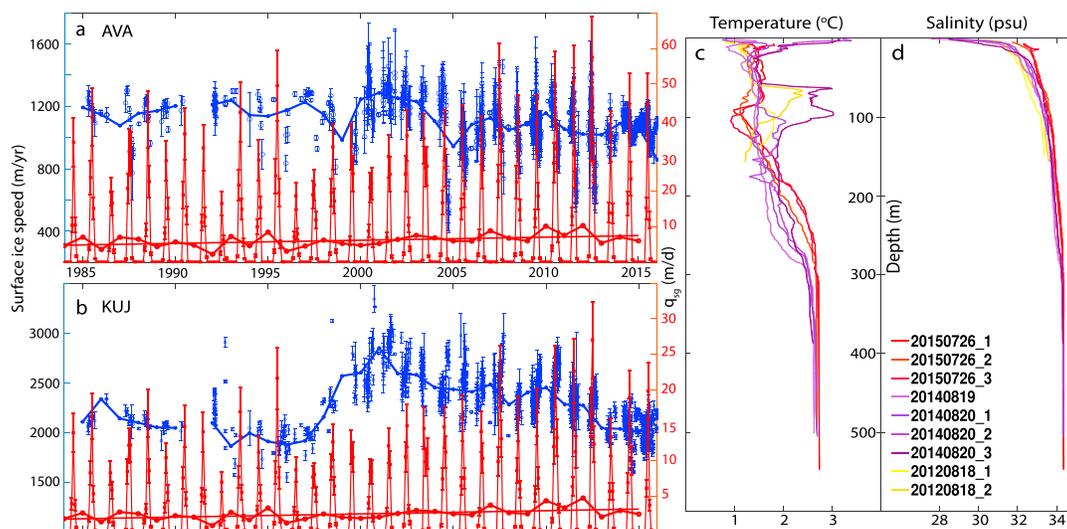
Figure 3. Time series of surface ice front velocity (m/yr) averaged over the glacier width (blue) from 1984 to 2017 and mean annual subglacial discharge (red) from RACMO2.3 (Ettema et al., 2010) from 1992 to 2015 for (a) Avannarleq (AVA) and (b) Kujalleq (KUJ), West Greenland. (c) Temperature and (d) salinity in Torssukatak Fjord derived from conductivity temperature depth (CTD) measurements collected in 2012, 2014, and 2015.

2.3. Airborne Gravity

On 16–27 August 2012, we conducted a helicopter-borne (Eurocopter AS-355 B2), high-resolution gravimetric survey using SGL's AIRGrav system. AIRGrav uses three orthogonal accelerometers and two 2-degrees-of-freedom gyroscopes mounted on an inertial platform (Argyle et al., 2000). The primary accelerometer is held within 10″ (0.0028°) of level by a Schuler tuned inertial platform to the local vertical (Sander et al., 2005). A Novatel OEM4 and OEMV GPS receivers and data loggers provide average position of the helicopter and raw range information at 10 Hz. Data resolution and accuracy depend on survey speed and height above ground (An et al., 2017). The survey was flown at an average speed of 56 knots or 29 m/s with a ground clearance of 80 m at a 500 m spacing grid (Figure 1) (An et al., 2017). SGL proprietary software was used for AIRGrav data processing. As the Gordon and Betty Moore Foundation (GBMF) funded the survey, we refer to the gravity data as the GBMF gravity data. We refer to the gravity data as the GBMF gravity data.

The GBMF gravity line data are processed with 20, 28, 36, and 42 s half-wavelength filters. These filters provide nearly identical gravity anomalies for the two glaciers, albeit with a reduced data noise for the longer filters. For the 3-D inversion, we use the 750 m gridded data, which offer the best compromise between data noise and spatial resolution. The precision of the AIRGrav data from an analysis of cross over is 0.5 mGal. For comparison, Operation IceBridge gravity data has a spatial resolution of 4.9 km (aircraft speed 262 knots or 135 m/s) using a 70 s full wavelength filter (Cochran & Bell, 2010), hence 1 order of magnitude coarser spatial resolution.

2.4. Surface Elevation

The helicopter carried a Riegl LD90-31K-HiP Infrared Laser Rangefinder with a range of 1,500 m, a resolution of 1 cm, an accuracy of 5 cm, and a data rate of 3.3 Hz. Comparing the GBMF laser elevation data with a digital elevation model from July 1985 (Korsgaard et al., 2016), we find that the surface elevation of AVA has not changed at a detectable level (±10 m) during that period (Figure S1 in the supporting information), which is consistent with the stability of its ice front position. For KUJ, the ice surface elevation dropped by 20 m in 29 years within a few kilometers of the ice front. Felikson et al. (2017) found that this thinning extends 15 km from the terminus.

2.5. MBES Survey

The first MBES survey was conducted in 2007 on board the R/V Maria S. Merian (Weinrebe et al., 2009) using a Kongsberg-Simrad EM120 system with data processed using the MB software. In August 2012, 2013, 2014, and 2015, we deployed a Reson 8160 MBES system operating at 50 kHz with a 3 km range on the "Esle" (2012) and "Cape Race" (2013–2014) (Rignot, Fenty, et al., 2016). The Reson was operated with a NAVCOM 3050 differential GPS unit with submeter position accuracy and an Applanix POS MV: Position & Orientation Systems for Marine Vessels. inertial navigation system, which provided real time vessel attitude and position. The data

were acquired using the QINSy software and processed using the CARIS HIPS software. Calibration of sound speed in water was performed using conductivity temperature depth data obtained at regular intervals during the cruise. In 2016, we employed a SeaBat 577 sonar on board the "Ivila." The MBES data were gridded at 25 m spacing with a nominal vertical precision of 2 m (Figure 1b).

2.6. Gravity Inversion

We form a 3-D model of AVA and KUJ using Geosoft GM-SYS 3-D software which implements the method of Parker (1973). The model included three horizontal layers: (1) a solid ice layer with a density of 0.917 g/cm^3, (2) a sea water layer with a density of 1.028 g/cm^3, and (3) a rock/sediment substrate layer with a uniform density of 2.60 g/cm^3 for AVA and 2.69 g/cm^3 for KUJ. The model domain extends to the limit of the GBMF survey. We allow a 500 m wide transition at the boundary where the inversion is modulated by a factor varying linearly between 0 (no gravity inversion) to 1 (full gravity inversion) as a function of distance from the gravity data. We invert the gravity data inside the inversion domain, which includes land ice and portions of the ocean not surveyed by MBES (inversion factor > 0). We calculate the DC shift of the gravity data (or mean gravity anomaly) where the MBES data overlap with the GBMF gravity data (An et al., 2017).

The initial solution uses the BM3 and MBES data with a linear interpolation in between. Outside of the survey domain, we simulate the gravity field using a forward model from GM-SYS 3-D to fill in the observational gaps. We match the gravity values at the boundary of the inversion using a 500 m wide transition boundary. During the inversion, the unknown bed elevation is modified iteratively until we obtain the best match between modeled and observed gravity. The iteration stops when the standard deviation of the misfit drops below 0.1 mGal. To provide an output product that preserves the resolution of MBES, we grid the inversion results at 25 m spacing (Figure 1b).

To define an optimal average density for the glacier bed and fjord depth, we calculate the rate of convergence of the solution between modeled and observed gravity for densities varying from 2.5 to 3.0 g/cm^3 with steps of 0.01 g/cm^3. We find a minimum at a density of 2.60 g/cm^3 for AVA and 2.69 g/cm^3 for KUJ (Figure S2). Such density is compatible with the presence of tonalite, granite, and sandstone in this area according to the Geological Survey of Denmark and Greenland (Pedersen et al., 2013).

2.7. Model Evaluation

We compare the gravity results with (1) BM3, (2) the bed topography from Bamber et al. (2013) B13 that grids Multichannel Coherent Radar Depth Sounder (MCoRDS) ice thickness data using kriging combined with the International Bathymetric Chart of the Arctic Ocean (IBCAO) version 3.0 (Jakobsson et al., 2012) (Figure S3), and (3) survey lines of MCoRDS RES data along the glacier centers collected on 14 April 2014 for AVA and 6 April 2013 for KUJ (Figure S4). To translate the gravity misfit of the solution into a bed elevation error, we calculate the gravity anomaly using GM-SYS 3-D obtained by shifting the bed solution by 100 m and compare the results with the original gravity field. We find an average shift of 5 mGal in gravity anomaly per 100 m of ice in the trough. This scaling factor is applied to the gravity misfit to derive an uncertainty in bed elevation in meters (Figure S5).

3. Results

The gravity anomalies within the survey domain vary from −95 mGal in the fjord to +35 mGal on surrounding mountain peaks, with peak negative values in the ocean and near the ice fronts (Figure 1a). The inferred bed depth is positively correlated with the gravity anomaly, as expected if the bed density was constant within the inversion domain (Figure 1b). The inversion reveals that the glaciers flow in troughs below sea level that form a ridge at the location of the ice fronts.

Torssukataq Fjord is 600–700 m deep, with a relatively flat bottom characteristic of fjord filled with glacier sediments (Figure 1b), until the seafloor rises abruptly by several hundreds of meters of 5 km of the ice fronts. For AVA, the seafloor is 560 m deep and 4 km from the ice front (Figure 2) and rises to 100–200 m at the ice front. The ice front stands on a ridge 2 km wide, varying from 300 m deep to the west to 100 m deep to the east. The western trough coincides with a channel of subglacial discharge observed every summer (Rignot et al., 2010). No outburst of subglacial water is visible in the east where the ridge is shallow. Upstream of the ridge, the bed follows a reverse slope and drops to 500 m depth in 6 km. Above km 4, AVA splits into two tributaries, 400 m deep to the west and 200 m to the east. Both tributaries remain several hundreds of meters below sea level beyond the inversion domain.

Comparing the AVA gravity results with MCoRDS, we find an excellent agreement in bed elevation and ice thickness. The root-mean-square error is 13 m from km 2 to km 10 in profile AA′. This agreement increases confidence in the inversion since the MCoRDS data are independent. In contrast, the BM3 solution is 100 m shallower between km 2 and km 6. We attribute the difference to uncertainties in BM3 discussed earlier. Compared with B13, the gravity solution is 200 to 300 m deeper between km 2 to km 6. The difference becomes less than 100 m above km 6. We attribute the errors in B13 to kriging of sparse observations. Our inferred bed uncertainty for AVA is ±37 m (Figure S5).

On KUJ, the bed rises from 600 m to 300 m in 3–4 km (Figures 2d–2f). Higher seafloor, at 300 m depth, coincides with the ice front location in the 1990s (1990–1996). A 1 km wide ridge underlaid the ice front at that time, 200 m deep on the north and south sides and 300 m at the center. Between km −1 and +1, our bed solution reveals a small reverse slope with an elevation dropping from 300 to 450 m depth in 3–4 km. The current ice front position stands in a flatter area at 400 m depth. Upstream of the 2017 ice front position, the bed rises by a few tens of meters over 1 km. This bump in elevation is apparent across the entire glacier but remains within the noise level of the inversion (±43 m in Figure 2f). At that location, no MCoRDS bed echo is detected. Compared to BM3, the gravity solution is 50 m deeper at km 0, with a more concave profile. The gravity solution agrees with the MCoRDS data within 10 m. In contrast, B13 incorrectly represents the glacier as land terminating.

We conclude that KUJ ice front is constrained by the presence of a sill that is narrower (1 km) and deeper (300 m) than AVA. KUJ retreated to a deeper, flatter position after the 1990s and has been stable since. AVA has been stable the entire past century on a shallower (100–200 m), wider (2 km) sill.

4. Discussion

The gravity solution reveals the presence of sills at the mouth of AVA and KUJ and deeper beds immediately upstream. Comparison with MCoRDS data at the center line (Figure 2c) suggests that the gravity solution is more reliable than BM3 which is affected by uncertainties in SMB, ice thinning, and sparse ice thickness data. AVA has no thickness data in the last 22 km versus 5 km for KUJ to constrain BM3.

The sill at the ice front of AVA has held the glacier position in place for 167 years (Weidick, 1968). A comparison of the ice front surface elevation with that required to reach hydrostatic equilibrium (HE) reveals an ice front standing 20–30 m above HE (Figure 2) using a digital elevation model from 1985 (Korsgaard et al., 2016) and WorldView from 2012. Joughin et al. (2012) observed that Jakobshavn Isbrρ maintained an ice cliff 20 m above HE during its entire retreat along a deeper bed. At the 20–30 m threshold, ice blocks are nearly free of basal friction, detach from the front, rotate, and roll away into the ocean. This form of calving produces the largest icebergs in Illulissat, Torssukatak, and other fjords (Holland et al., 2016; Joughin et al., 2008). As ice advances past the sill of AVA, the bed elevation drops rapidly, the threshold is easily exceed, and ice blocks calve to maintain a stable calving front.

For KUJ, the ice front was at the sill in the early part of the twentieth century, retreated to a deeper, flatter position by the midtwentieth century, readvanced in the 1960s to 1980s, before retreating again in the late 1990s. As the glacier retreated into a deeper bed with a reverse slope, it sped up by 23%. Following that speedup, the glacier has slowed down progressively to return to its prior speed around 2015. The glacier has overall experienced modest retreat since 1851 (Weidick, 1968). The sill has stabilized the calving front in prior times. At the 1985 ice front, the ice surface was 20 m above HE and hence prone to ice block rotation. In 2012, the surface was 40 m above HE, hence in a similar favorable situation but with thicker ice blocks. In between the current front and the sill, icebergs and debris jam up the ice front since the sea floor rises away from the ice front. We observe more ice jamming in front of KUJ than AVA. In Southwest Greenland, a similar setting has controlled the stability of Kangiata Nunaata Sermia (Motyka et al., 2017).

Conductivity temperature depth collected in the fjord reveals the presence of warm AW below 300–350 m depth (Figure 3). The major portion of the corresponding ocean heat does not reach the glacier front because a sill depth at 300 m for KUJ and AVA. We calculate a thermal forcing of 3.87°C at 300 m in 2012–2015. We use a reconstruction of temperature from Rignot et al. (2012) to estimate an ocean thermal forcing in Disko bay of 1.6°C in the 1990s. Ocean waters warmed up by 2.0°C from the 1990s to 2000s (Holland et al., 2008; Rignot et al., 2012) and another 0.27°C in 2012–2015. We estimate the rate of ice front undercutting by the ocean using the parameterized model of Rignot, Xu, et al. (2016). The average water depth at the glacier front is 131 m

for AVA and 311 m for KUJ. The average subglacial discharge, q_{sg}, derived from RACMO2.3 doubled from 4.7 m/d in the 1990s to 6.5 m/d in the 2000s and 7.8 m/d in 2010s for AVA versus 1.8 to 2.6 and 3.4 m/d for KUJ. The resulting rate of ice front undercutting, q_m, tripled from 0.4 to 1.0 and 1.2 m/d for AVA and 0.5 to 1.3 and 1.4 m/d for KUJ.

While this increase in q_m has been significant, the rate of ice advection, q_f, was 3.2 m/d for AVA and 5.7 m/d for KUJ in 1998, or 8 times greater than q_m for AVA and 3 times greater for KUJ. The glaciers were therefore dominated by dry calving processes, especially AVA, that is, by the advection of ice from upstream breaking into icebergs. As KUJ retreated, q_f increased to 7.0 m/d in the mid-2000s and q_m increased to 2.6 m/d. The glacier then found a more stable position. In 2012–2017, q_f dropped to 5.7 m/d, q_m increased to 3.4 m/d, so the ratio dropped to 1.7 for KUJ versus 2.7 in 2000, indicating the end of a dominance by dry calving processes for KUJ. For AVA, the ratio dropped to 2.3 in 2012–2017, which is a larger drop from the eightfold ratio in the 1990s. We conclude that both glaciers have become more vulnerable to ocean warming and could be dislodged from their stable position in the near future.

This work demonstrates the value of airborne gravity to resolve remaining gaps in the thickness of marine-terminating glaciers near ice fronts choked with iceberg debris to obtain a seamless mapping necessary to understand the glacier evolution. Our bed mapping is of sufficient quality ($\pm$30–40 m or better than 10%) to enable conceptual and numerical modeling of its past, recent, and future behavior in response to climate change. Prior mappings such as B13 had large errors (many 100 m or 100%) and did not reveal the presence of sills or ocean waters at the front and therefore could not explain the glacier behavior. We recommend that a similar approach using high-resolution gravity data be employed in other major remaining fjords of Greenland, including the Kangerdlussuaq and Helheim glaciers in East Greenland and Kakiffaat Sermiat in North West Greenland among others as an essential prerequisite to interpretation and modeling of their dynamics.

5. Conclusions

High-resolution airborne gravity acquired at a low aircraft speed, with low ground clearance, combined with novel multibeam echo sounding data of the fjord helps resolve the bed topography and ice thickness of major outlet glaciers flowing into the ice-chocked Torssukatak Fjord in central West Greenland. The results explain the exceptional stability of two large glaciers over the last 1.5 century, despite the presence of warmer ocean waters in the fjord since the mid-1990s, because the glaciers are protected from the ocean by sills at the end of deep (700 m) fjords. The retreat of these glaciers from the deep fjords to the sills precedes year 1851. Resolving the bed topography and fjord depth of all marine-terminating glaciers controlling the ice discharge of the Greenland Ice Sheet shall remain a priority to understand, model, and predict the evolution of glaciers in a changing climate.

References

An, L., Rignot, E., Elieff, S., Morlighem, M., Millan, R., Mouginot, J., et al. (2017). Bed elevation of Jakobshavn Isbrae, West Greenland, from high-resolution airborne gravity and other data. *Geophysical Research Letters*, *44*, 1–9. https://doi.org/10.1002/2017GL073245

Argyle, M., Ferguson, S., Sander, L., & Sander, S. (2000). AIRGrav results: A comparison of airborne gravity data with GSC test site data. *The Leading Edge*, *19*(10), 1134–1138. https://doi.org/10.1190/1.1816088

Bamber, J. L., Griggs, J. A., Hurkmans, R. T. W. L., Dowdeswell, J. A., Gogineni, S. P., Howat, I., et al. (2013). A new bed elevation dataset for Greenland. *Cryosphere*, *7*(2), 499–510. https://doi.org/10.5194/tc-7-499-2013

Carbonnell, M., & Bauer, A. (1968). Exploration des couvertures photographiques aeriennes repetees du front des glaciers velant dans Disko Bugt et Umanak Fjord. *Medd Gronland*, *173*(5), 78.

Cochran, J. R., & Bell, R. E. (2010). IceBridge Sander AIRGrav L1B geolocated free air gravity anomalies, Version 1, NASA National Snow and Ice Data Center. https://doi.org/10.5067/R1RQ6NRIJV89

Ettema, J., Van Den Broeke, M. R., Van Meijgaard, E., Van De Berg, W. J., Box, J. E., & Steffen, K. (2010). Climate of the Greenland ice sheet using a high-resolution climate model — Part 1: Evaluation. *Cryosphere*, *4*(4), 511–527. https://doi.org/10.5194/tc-4-511-2010

Felikson, D., Bartholomaus, T. C., Catania, G. A., Korsgaard, N. J., Kjær, K. H., Morlighem, M., et al. (2017). Inland thinning on the Greenland ice sheet controlled by outlet glacier geometry. *Nature Geoscience*, *10*(5), 366–369. https://doi.org/10.1038/ngeo2934

Gogineni, S., Yan, J. B., Paden, J., Leuschen, C., Li, J., Rodriguez-Morales, F., et al. (2014). Bed topography of Jakobshavn Isbræ, Greenland, and Byrd Glacier, Antarctica. *Journal of Glaciology*, *60*(223), 813–833. https://doi.org/10.3189/2014JoG14J129

Holland, D., Voytenko, D., Christianson, K., Dixon, T., Mei, M., Parizek, B., et al. (2016). An intensive observation of calving at Helheim Glacier, East Greenland. *Oceanography*, *29*(4), 46–61. https://doi.org/10.5670/oceanog.2016.98

Holland, D. M., Thomas, R. H., de Young, B., Ribergaard, M. H., & Lyberth, B. (2008). Acceleration of Jakobshavn Isbræ triggered by warm subsurface ocean waters. *Nature Geoscience*, *1*(10), 659–664. https://doi.org/10.1038/ngeo316

Jakobsson, M., Mayer, L., Coakley, B., Dowdeswell, J. A., Forbes, S., Fridman, B., et al. (2012). The International Bathymetric Chart of the Arctic Ocean (IBCAO) Version 3.0. *Geophysical Research Letters*, *39*, L12609. https://doi.org/10.1029/2012GL052219

Joughin, I., Howat, I., Alley, R. B., Ekstrom, G., Fahnestock, M., Moon, T., et al. (2008). Ice-front variation and tidewater behavior on Helheim and Kangerdlugssuaq Glaciers, Greenland. *Journal of Geophysical Research*, *113*, F01004. https://doi.org/10.1029/2007JF000837

Joughin, I., Smith, B. E., Howat, I. M., Floricioiu, D., Alley, R. B., Truffer, M., & Fahnestock, M. (2012). Seasonal to decadal scale variations in the surface velocity of Jakobshavn Isbrae, Greenland: Observation and model-based analysis. *Journal of Geophysical Research*, *117*, F02030. https://doi.org/10.1029/2011JF002110

Korsgaard, N. J., Nuth, C., Khan, S. A., Kjeldsen, K. K., Bjørk, A. A., & Kjær, K. H. (2016). Digital Elevation Model and orthophotographs of Greenland based on aerial photographs from 1978–1987. *Scientific Data*, *3*, 1–15. https://doi.org/10.1038/sdata.2016.32

Krabill, W. (2000). Greenland ice sheet: High-elevation balance and peripheral thinning. *Science*, *289*(5478), 428–430. https://doi.org/10.1126/science.289.5478.428

Luckman, A., & Murray, T. (2005). Seasonal variation in velocity before retreat of Jakobshavn Isbræ, Greenland. *Geophysical Research Letters*, *32*, L08501. https://doi.org/10.1029/2005GL022519

Lüthi, M. P., Vieli, A., Moreau, L., Joughin, I., Reisser, M., Small, D., & Stober, M. (2016). A century of geometry and velocity evolution at Eqip Sermia, West Greenland. *Journal of Glaciology*, *62*(234), 640–654. https://doi.org/10.1017/jog.2016.38

Meier, M. F., & Post, A. (1987). Fast tidewater glaciers. *Journal of Geophysical Research*, *92*(B9), 9051–9058. https://doi.org/10.1029/JB092iB09p09051

Morlighem, M., Rignot, E., Mouginot, J., Seroussi, H., & Larour, E. (2014). Deeply incised submarine glacial valleys beneath the Greenland ice sheet. *Nature Geoscience*, *7*(6), 18–22. https://doi.org/10.1038/ngeo2167

Morlighem, M., Williams, C. N., Rignot, E., An, L., Arndt, J. E., Bamber, J. L., et al. (2017). BedMachine v3: Complete bed topography and ocean bathymetry mapping of Greenland from multibeam echo sounding combined with mass conservation. *Geophysical Research Letters*, *44*, 11,051–11,061. https://doi.org/10.1002/2017GL074954

Motyka, R. J., Cassotto, R., Truffer, M., Kjeldsen, K. K., Van As, D., Korsgaard, N. J., et al. (2017). Asynchronous behavior of outlet glaciers feeding Godthåbsfjord (Nuup Kangerlua) and the triggering of Narsap Sermia's retreat in SW Greenland. *Journal of Glaciology*, *63*(238). https://doi.org/10.1017/jog.2016.138

Parker, R (1973). The rapid calculation of potential anomalies. *Geophysical Journal International*, *31*(4), 447–455.

Pedersen, M., Weng, W. L., Keulen, N., & Kokfelt, T. F. (2013). A new seamless digital 1:500 000 scale geological map of Greenland. *Geological Survey of Denmark and Greenland Bulletin*, 65–68.

Pfeffer, W. T. (2007). A simple mechanism for irreversible tidewater glacier retreat. *Journal of Geophysical Research*, *112*, F03S25. https://doi.org/10.1029/2006JF000590

Rignot, E., Fenty, I., Menemenlis, D., & Xu, Y. (2012). Spreading of warm ocean waters around Greenland as a possible cause for glacier acceleration. *Annals of Glaciology*, *53*(60), 257–266. https://doi.org/10.3189/2012AoG60A136

Rignot, E., Fenty, I., Xu, Y., Cai, C., Velicogna, I., Cofaigh, C., et al. (2016). Bathymetry data reveal glaciers vulnerable to ice-ocean interaction in Uummannaq and Vaigat glacial fjords, West Greenland. *Geophysical Research Letters*, *43*, 2667–2674. https://doi.org/10.1002/2016GL067832

Rignot, E., Koppes, M., & Velicogna, I. (2010). Rapid submarine melting of the calving faces of West Greenland glaciers. *Nature Geoscience*, *3*(3), 187–191. https://doi.org/10.1038/ngeo765

Rignot, E., & Mouginot, J. (2012). Ice flow in Greenland for the International Polar Year 2008–2009. *Geophysical Research Letters*, *39*, L11501. https://doi.org/10.1029/2012GL051634

Rignot, E., Xu, Y., Menemenlis, D., Mouginot, J., Scheuchl, B., Li, X., et al. (2016). Modeling of ocean-induced ice melt rates of five West Greenland glaciers over the past two decades. *Geophysical Research Letters*, *43*, 6374–6382. https://doi.org/10.1002/2016GL068784

Sander, S., Argyle, M., Elieff, S., Ferguson, S., Lavoie, V., & Sander, L. (2005). The AIRGrav airborne gravity system. *CSEG Recorder*, *30*(8), 32–36.

Straneo, F., Heimbach, P., Sergienko, O., Hamilton, G., Catania, G., Griffies, S., et al. (2013). Challenges to understanding the dynamic response of Greenland's marine terminating glaciers to oceanic and atmospheric forcing. *Bulletin of the American Meteorological Society*, *94*(8), 1131–1144. https://doi.org/10.1175/BAMS-D-12-00100.1

Thomas, H., Akins, L., Csatho, M., Frederick, E. B., Krabill, B., Manizade, S., & Rignot, E. J. (2000). Substantial thinning of a major east Greenland outlet glacier. *Geophysical Research Letters*, *27*(9), 1291–1294.

Thomas, R. H. (1979). The dynamics of marine ice sheets. *International Glaciological Society*, *24*(90), 167–177. https://doi.org/10.1017/S0022143000014726

van den Broeke, M., Bamber, J., Ettema, J., Rignot, E., Schrama, E., van de Berg, W. J., et al. (2009). Partitioning recent Greenland mass loss. *Science*, *326*(5955), 984–986. https://doi.org/10.1126/science.1178176

Weertman, J. (1974). Stability of the junction of an ice sheet and an ice shelf. *Journal of Glaciology*, *13*(67), 3–11. https://doi.org/10.3198/1974JoG13-67-3-11

Weidick, A. (1968). Observations on some Holocene glacier fluctuations in West Greenland. *Meddelelser om Grønland*, *164*(6), 212.

Weinrebe, W., Kuijpers, A., Klaucke, I., & Fink, M. (2009). Multibeam bathymetry surveys in fjords and coastal areas of West-Greenland. In Abstract OS21A-1152 Presented at the 2009 AGU Fall Meeting, San Francisco, CA.

Erratum

In the originally published version of this article, there were two typographical errors in Figure 2. In Figure 2a, the "0" position was misplaced in the bed elevation legend; in Figure 2c, the second dark "Δ" on the x axis was misplaced. These errors have since been corrected, and the present version may be considered the authoritative version of record.